



## Synthesis, characterization of titania supported on mesoporous MCM-41 and its application for the removal of methylene blue

Reda. S. Salama<sup>1\*</sup>, Sohier. A. El-Hakam<sup>2</sup>, Salem. E. Samra<sup>2</sup>, Shady. M. El-Dafrawy<sup>2</sup>, Amr Awad Ibrahim<sup>2</sup>, and Awad I. Ahmed<sup>2</sup>

<sup>1</sup> Basic Science Department, Faculty of Engineering, Delta University for Science and Technology, Gamasa, Egypt

<sup>2</sup> Chemistry Department, Faculty of science, Mansoura University, Mansoura, Egypt

\* Corresponding author at: Basic Science Department, Faculty of Engineering, Delta University for Science and Technology, Gamasa, Egypt., Tel.: +201061391656; e-mail address: [reda.salama@deltauniv.edu.eg](mailto:reda.salama@deltauniv.edu.eg), [dr.reda.salama@gmail.com](mailto:dr.reda.salama@gmail.com) (R. S. Salama).

### ABSTRACT

Solid acid substance of MCM-41 prepared by sol-gel method followed by incorporation of TiO<sub>2</sub> within the mesochannels through a simple and effective impregnation method. TiO<sub>2</sub> loaded on MCM-41 were synthesized at room temperature using tetraethoxysilane (TEOS), Cetyltrimethylammonium bromide (CTAB) as template and titanium (IV) isopropoxide (TIP) as titanium source. The resultant mesoporous TiO<sub>2</sub>/MCM-41 samples were calcined at 550 °C. The resultant samples were characterized using X-ray diffraction patterns (XRD), BET measurements, FT-IR and high-resolution transmission electron microscopy (TEM). Nitrogen adsorption-desorption measurements were used to measure surface area and average pores diameter at -196°C. The TiO<sub>2</sub>/MCM-41 with higher Ti/Si ratio shows low structural integrity and the formation of Ti-oxide species leading to a considerable decrease in surface area. The activities of TiO<sub>2</sub>/MCM-41 for adsorption of methylene blue (MB) studied in details. Adsorption increase with the modification of MCM-41 by TiO<sub>2</sub> up to 25% of TiO<sub>2</sub> then decreased. The samples of 25% TiO<sub>2</sub> loaded on MCM-41 show higher catalytic activity.

**Keywords:** TiO<sub>2</sub> loaded MCM-41; sol-gel; TEOS; water treatment; Methylene Blue.

### 1. Introduction

In recent years, environmental considerations have raised strong interest in the development of economically feasible materials and processes to eliminate the use of harmful substances and the generation of toxic waste materials. In this respect, heterogeneous catalysis can play a key role in the development of environmentally benign processes. For examples, many industries use dyes to color their products and also consume large volumes of water. The presence of tiny amounts of dyes in water is highly visible and undesirable (Alshorifi et al., 2021). The removal of dyes from wastewaters is of a great concern nowadays, because many dyes and their degradation products are toxic and carcinogenic, posing a serious risk to aquatic organisms (Crini, 2006). Methylene blue (MB) is the most commonly used for dyeing cotton, wood and silk. Although the dye is not regarded as a very toxic dye, MB can have various harmful effects on animals and human beings. Once inhaled, it can cause vomiting, nausea and heart rate increasing. Therefore, many methods are available for the removal of dyes from industrial effluents. The most widely used are biodegradation (El-Sheekh et al., 2009), flocculation-coagulation (Cañizares et al., 2006), photo catalysis (El-Hakam et al., 2022; El-Yazeed et al., 2022; Mannaa et al., 2021b) and adsorption (El-Hakam et al., 2021, 2018; Mannaa et al., 2021a; Reda S. Salama et al., 2021b; Salama, 2019). Among these methods, adsorption technique has been proven to be effective and attractive for the treatment of dye-bearing wastewaters. Adsorption is also a comparatively cheap and effective method in the removal of MB dyes. The adsorption characteristics of MB dyes on different adsorbents, such as activated carbon (AC), agriculture waste, industrial solid wastes, clay, sewage sludge, silica (El-Hakam et al., 2013a; Reda S Salama et al., 2021) etc. have been extensively investigated. Among these adsorbents, silica (MCM-41) and titania-silica adsorbents widely used as adsorbent for the MB's removal (El-Hakam et al., 2018; Mannaa et al., 2021b).

MCM-41 has become one of the most popular mesoporous molecular sieves in the family of M41S, which was disclosed in 1992 by Mobil oil Corporation (Ibrahim et al., 2021; Jermy and Pandurangan, 2008). Due to its unique properties, e.g., well defined mesostructure, narrow pore size distribution, tunable pore diameter and high specific surface areas, MCM-41 has been widely used in heterogeneous catalysis, separation, optical fields as well as gas adsorption (El-Hakam et al., 2013a, 2013b; Reda S. Salama et al., 2021a). Due to the large surface area and nanometer sized pore of the mesoporous compounds, especially MCM-41 been believed the promising materials as adsorbents for various inorganic ions and organic dyes. However, MCM-41 in its pure siliceous form shows limited applications, so, modification is necessary by incorporating active components into the MCM-41 framework such as transition metal complexes can be supported (Chen et al., 2009). Aronson et al. (Aronson et al., 1997) have grafted TiO<sub>2</sub> nanoparticles into the mesopores of MCM-41 by introducing TiCl<sub>4</sub> in hexane in the presence of a surfactant. However, both rutile and anatase phases were formed on the external surface as minor and major phases respectively. Since, the handling of toxic chemicals such as TiCl<sub>4</sub> is hazardous, the use of eco-friendly chemicals is significant as far as pollution and handling is concerned. Titania can be incorporated into the silica structure by direct or post-synthesis methods resulting in different types of isolated or bulky active sites on the surface of mesopore walls or in the channels, respectively. TiO<sub>2</sub> modified MCM-41 mesoporous silica has been investigated as photocatalysts (Shi et al., 2011) or solid acid catalysts in some reactions, such as transesterification (Eimer et al., 2008). It has an extensive application prospect in functional ceramics, sensor materials, cosmetics products and high-grade coatings. Studies on the reactions catalyzed by TiO<sub>2</sub>-modified-MCM-41 have focused on the relationship between the acidity and catalytic performance.

Here we report the formation of MCM-41 and TiO<sub>2</sub> nanoparticles in the pores of Si-MCM-41. We have used Ti (IV) isopropoxide as the source of titanium and isopropanol as a medium for the incipient wetness impregnation method then characterized firstly for their adsorption properties by nitrogen adsorption at -196°C to determine total pores, micropore and mesopores volume, surface area and average pore diameter. Secondly for their surface chemistry by FT-IR, acidity measurements, XRD, and TEM images. It has been observed that the titania particles are bonded to the silica network, which controls the particle size of titania. After preparation and characterization, find out the possibility of using such adsorbent for removal of methylene blue dye in aqueous solution then the equilibrium and kinetic data of the adsorption were studied to understand the adsorption.

## 2. Material and methods

### 2.1. 2.1 Materials

All inorganic and organic chemicals used in preparation of adsorbent are: Cetyltrimethylammonium bromide (CTAB), tetraethoxysilane (TEOS), ammonia hydroxide solution (33%), Titanium (IV) isopropoxide (TIP), isopropanol and methylene blue (MB).

### 2.2 2.2 adsorbent preparation

The original method for preparation of MCM-41 was first proposed by Beck et al [8]. However, the method used here is based on the modifications introduced in the original method to conduct the synthesis in mild conditions in terms of temperature and amount of surfactant amount. In a typical synthesis [29], 2.0 g of Cetyltrimethylammonium bromide (CTAB) was completely dissolved in 120 ml of distilled water at room temperature then 12.5 ml of aqueous ammonia was added to this solution. After that, 10 ml of tetraethoxysilane (TEOS) was added to the solution under vigorous stirring. At higher tetraethoxysilane loading, a thick white paste is formed. The product was filtered, washed with distilled water and dried in air at 120°C. The mole composition of the gel mixture was CTAB: TEOS: ammonia: H<sub>2</sub>O = 0.22: 1.04: 1.39: 44.4. The mesoporous material was finally obtained by calcination of the hybrid structure at 550°C for 6h.

TiO<sub>2</sub> was supported on MCM-41 by an impregnation method. Amount of calcined MCM-41 was dispersed under vigorous stirring into a solution of the desired amount of Titanium (IV) isopropoxide (TIP) as titanium source in 10 ml of isopropanol and impregnated for 24h. The TiO<sub>2</sub> contents were taken to be 2%, 8%, 15%, 25%, 35% and 45%. The product was filtered using rotary at 70°C to evaporate isopropanol. The resultant is calcined in muffle at 550°C in presence of air for 2 h.

### 2.3. Characterization

XRD patterns of all samples were scanned at  $2\theta$  angle from 1 to 70 using PW 150 (Philips) using Cu K $\alpha$  radiation source and Ni filter. The apparatus was operated at 40 kV and 45mA. The average crystallite size of particles was determined by Scherer's formula ( $D = 0.9 \lambda / \beta \cos\theta$ ) where  $\lambda$  is radiation wavelength ( $\text{\AA}$ ),  $\beta$  is the line breadth (radians) and  $\theta$  = angle of reflection. The specific surface areas, average pore diameter and pore size distribution of the calcined samples were determined from nitrogen adsorption-desorption studied conducted at 77 K using the high vacuum conventional volumetric glass system. Transmission electron microscopy image and particle size were obtained using a Philips CM120 Biotwin electron microscope operating at 120 KV. TEM samples were prepared by dipping an alcohol suspension of fine sample powders onto a Copper grid coated with holey

Carbon foil and dried at ambient temperature. The IR spectra of modified Titania loaded on MCM-41 with different titania content were recorded with Nicolet Magna-IR 550 spectrometer with a 4 cm<sup>-1</sup> resolution and 128 scans in the mid-IR region 400-4000 cm<sup>-1</sup>. The sample was ground with KBr and pressed into a thin wafer that was placed inside the IR cell and then the spectrum was recorded.

#### 2.4. adsorption activity (*Adsorption of methylene blue (MB)*)

The well-known methylene blue cationic dye (MB) is commonly used to probe the mesoporous volume of activated MCM-41 and TiO<sub>2</sub> loaded on MCM-41 by adsorption experiments. Adsorption studies were carried out with 100 mg of activated adsorbent introduced into 100 ml of methylene blue (MB) solutions with different initial concentration in the range 0-150 mg/L. The pH of suspension was adjusted to 8-10 using 0.1 M HCl and 0.1 M NaOH solution. The adsorption equilibrium of MB on the prepared materials was reached after 4 hr of stirring at 25°C and 250 rpm. The suspensions were filtered, and then methylene blue (MB) equilibrium concentrations were determined by spectrophotometer at 665 nm. The adsorbed amount of MB at equilibrium ( $q_e$  in mg/g), was calculated by the following equation:

$$q_e = \frac{[(C_0 - C_e)V]}{Wt}$$

Where  $C_0$  is the initial dye concentration (mg/L),  $C_e$  is the equilibrium dye concentration (mg/L),  $V$  (L) is the volume of solution (100 ml) and  $wt$  (g) is the weight of the adsorbent. Two famous isotherms equations, namely Langmuir isotherm and Freundlich isotherm (Freundlich, 1907) were applied to fit the experimental data of MB adsorption.

### 3. Results and discussions

#### 3.1. X-ray diffraction patterns (XRD)

Low angle XRD profiles of different weight content of TiO<sub>2</sub> loaded on MCM-41 samples are presented in Fig 1. The MCM-41 sample shows a well-defined hexagonal structure, which is evidenced by the diffraction peaks at 2.3°, 4.0° and 4.8° assignable to the (100), (110) and (200) silica planes, respectively (Do et al., 2005). However, a decrease in the structural regularity is observed upon the loading of TiO<sub>2</sub>. This sample exhibits a poorly defined XRD pattern which may be due to the partial collapse as well as to the block of the mesochannels pores produced by the loading of TiO<sub>2</sub> (Do et al., 2005). The main difference between pure MCM-41 and TiO<sub>2</sub>-MCM-41(TM) with different Ti-oxide content is the intensity of TiO<sub>2</sub>/MCM-41 diffraction peaks decreased obviously with increasing the TiO<sub>2</sub> content, the reason lies in two kinds: one is due to pore filling of the host material, which reduces the scattering contrast between pore walls and pores, thus leading to a reduce in peak intensity, the higher the electron density of the sorbate molecule, the lower the residual peak intensity in the powder diffraction diagram (Bandyopadhyay et al., 2005). The other reason is that the decrease of peak intensity with successive loading of metal salt may be attributed to loss of sample integrity (Parala et al., 2000). But in this experiment, the decrease of diffraction peak is possibly caused by the first reason.

The wide-range X-ray diffraction patterns were obtained by scanning the samples from 10 to 75 degrees as presented in Fig 2. Which exhibits a number of peaks at  $2\theta = 25.4^\circ, 37.8^\circ, 48^\circ$  and  $54.4^\circ$ , which assigned to anatase phase which the intensity of it increased by increase the amount of TiO<sub>2</sub> content, also the peaks at  $48^\circ$  and  $54.4^\circ$  become more visible with increase in TiO<sub>2</sub> content. These results are agreement with the results of Hsien and Coworkers (Hsien et al., 2001), who prepared Titania modified MCM-41 by impregnation method. The addition of Titania into MCM-41 changes the crystal phase structure. The increase in TiO<sub>2</sub> content resulted in an increase in the degree of crystallization that can be noticed from the increasing of peak intensities as shown in Fig 2. The crystallite size  $D_{101}$  of tetragonal phase for some the selected samples was calculated using Scherrer equation (Ahmed et al., 2013).

$$D_{101} = \frac{0.9\lambda}{B_{101} \cdot \cos\theta}$$

Where  $\lambda$  is the wave length used and  $B_{101}$  is the full width at half maximum of the (101) peak at  $2\theta = 25.4^\circ$  which attribute for tetragonal phase. Crystallite size of the tetragonal phase line at  $2\theta = 25.2^\circ$  of (101) reflex for the selected samples is summarized in table 1, which shows the effect of TiO<sub>2</sub> content on crystallite size of MCM-41. Examination of Fig 2 shows that pure MCM-41 is amorphous and by addition of TiO<sub>2</sub> was associated with a notable increase of crystallite size to reach 25.9 nm for 25% TiO<sub>2</sub>/MCM-41 and 28.66 nm for 45% TiO<sub>2</sub>/MCM-41 as shown in table 1.

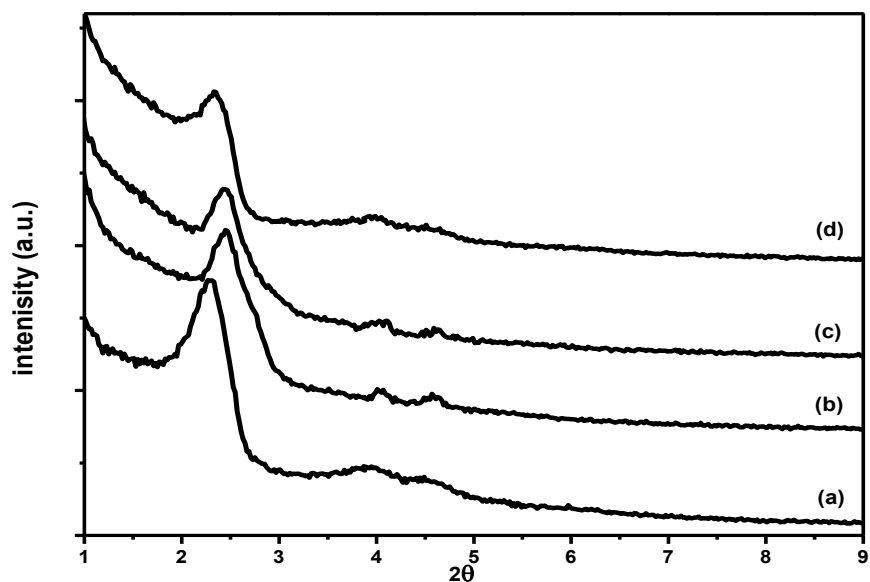


**Fig 1:** Small angle X-ray diffraction patterns of the calcined adsorbents at 550°C for (a) Pure MCM-41, (b) 2%, (c) 25% and (d) 45% TiO<sub>2</sub> loaded on MCM-41.

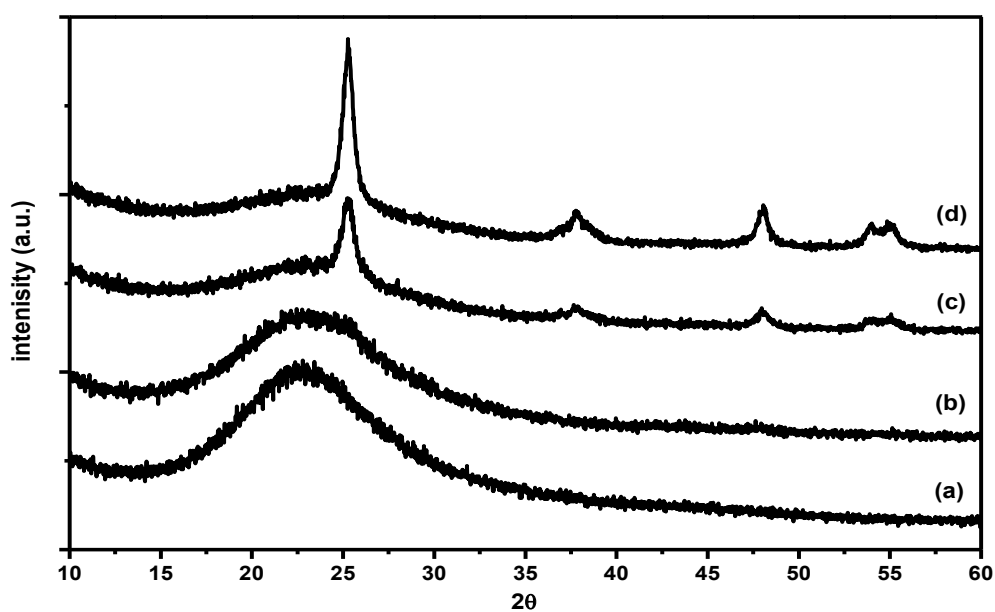


**Fig 2:** Wide angle X-ray diffraction patterns of the calcined adsorbents at 550°C for (a) Pure MCM-41, (b) 2%, (c) 25% and (d) 45% TiO<sub>2</sub> loaded on MCM-41.

**Table 1:** physicochemical properties and crystallite size of adsorbents (TiO<sub>2</sub>/MCM-41).

Sample name	d <sub>100</sub> (nm)	Unit cell a <sub>0</sub> (nm)	Crystallite size D (nm)
Pure MCM-41	3.61	4.168	Amorphous
2% TiO <sub>2</sub> /MCM-41	3.44	3.972	Amorphous
25% TiO <sub>2</sub> /MCM-41	3.407	3.934	25.92
45% TiO <sub>2</sub> /MCM-41	3.469	4.006	28.66

### 3.2. Nitrogen adsorption/desorption isotherms

The textural properties of materials such as surface area, pore volume, pore size distribution and pore geometry were determined for the prepared calcined samples from the low temperature adsorption of nitrogen at  $-196^{\circ}\text{C}$ . Moreover, the technique also discloses to what extent the measured surface area is associated with micro-, meso- and/or macropores. The most reliable information about the mesoporous structure of solids comes from low-temperature  $\text{N}_2$  adsorption isotherms. The mesoporous materials exhibit type IV isotherms of BDDT classification (Ahmed et al., 2013); this type has inflection around  $P/P_0 \sim 0.20-0.40$  with narrow hysteresis loops, which is characteristic of mesoporous materials with pore diameter in the range 2.0–4.0 nm (Lassaletta et al., 1996). Fig 3 to Fig 5 show the  $\text{N}_2$  adsorption–desorption isotherms at 77K of the samples. Little difference could be observed between the  $\text{N}_2$  sorption curves of mesoporous MCM-41 and those of metal deposited  $\text{TiO}_2$ -MCM-41. Suggesting that the introduced titania do not affect the mesoporous structure of MCM-41. Importantly, in most of the isotherms, it reveals that the titania diffuses through the entire pores, rather than agglomerate at the opening of the mesopores associated with “ink bottle” shaped pores, which shows more  $\text{H}_2$  character. Table 2 and Fig 6 show effect of  $\text{TiO}_2$  content on the surface area of MCM-41 sample. Pure MCM-41 calcined at  $550^{\circ}\text{C}$  showed a surface area of  $1378 \text{ m}^2/\text{g}$ . Addition of titania to the support results in a decrease in the surface area. The reduction in surface area after loading could be due to the fact that the  $\text{TiO}_2$  is deposited inside the mesochannels and is well dispersed on the surface of the hexagonally ordered mesoporous MCM-41 support. The surface area per gram of the support indicated that the loading of titania gradually decreased the surface area as shown in Fig 6. Table 2 and Fig 7 show the effect of calcination temperature on surface area of 25%  $\text{TiO}_2/\text{MCM-41}$ , This indicates that with the raise of the calcination temperature from  $450^{\circ}\text{C}$  to  $650^{\circ}\text{C}$ , is associated with some sort of sintering in which particle–particle adhesion may take place and leads to a decrease in the surface area (Radwan et al., 2005) as shown in Fig 7. The estimated values of  $S_{\text{BET}}$  are in good agreement with that of  $\alpha_s$ . This reveals the validity of both methods, i.e., BET and  $\alpha_s$  – methods used for the estimation of surface area. The different between  $S_{\text{BET}}$  and  $\alpha_s$  does not exceed 3% in some cases. The pore size distribution of pure and loaded MCM-41 shows a unique peak centered at about  $30^{\circ}\text{\AA}$  diameters as shown in Fig 8. It is evident that the pore volume and the specific surface area of the loaded sample are much lower compared to that of the pure MCM-41. This is consistent with previous results shown in table 2, the reduction in the pore volume and surface area after loading could be due to the fact that the  $\text{TiO}_2$  is deposited inside the mesochannels and is well dispersed on the surface of the hexagonally ordered mesoporous MCM-41 support.

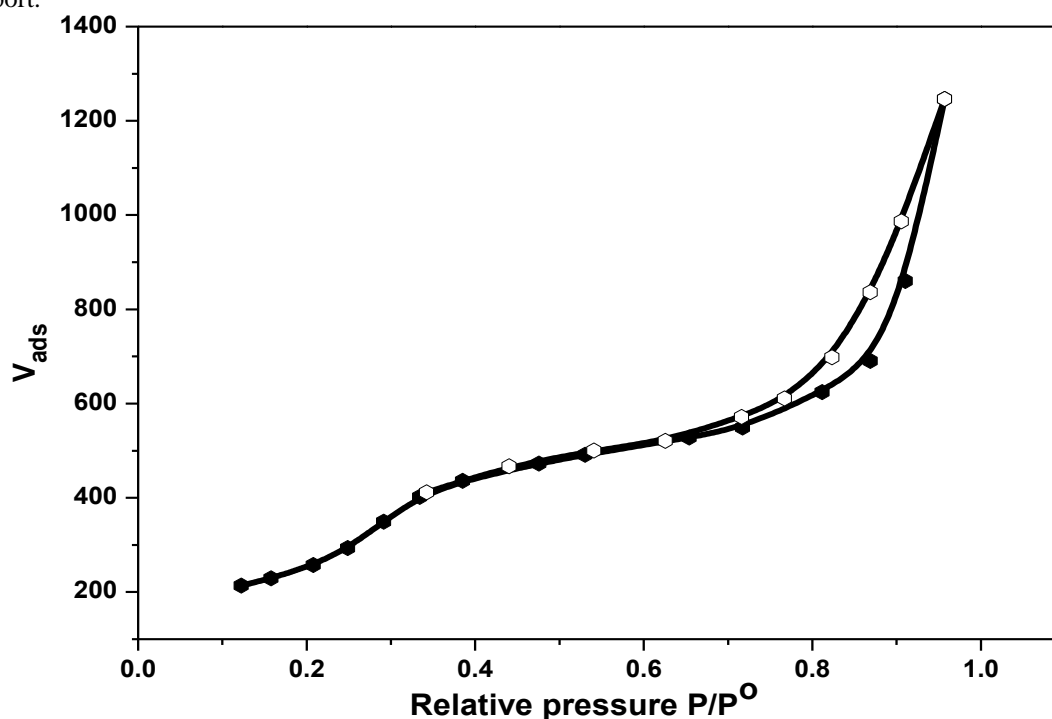
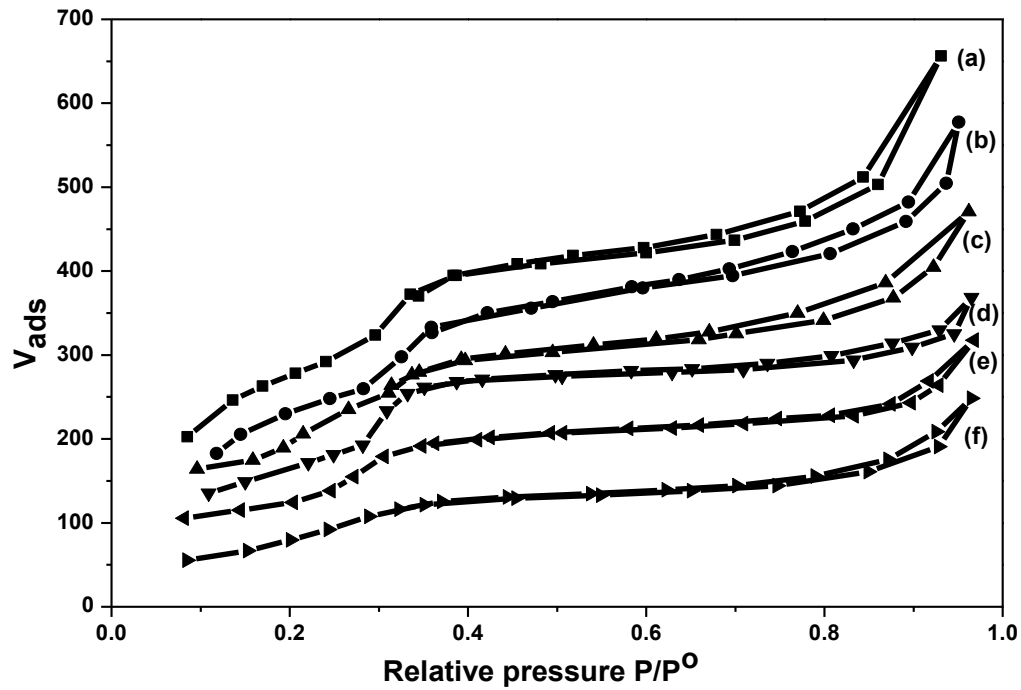
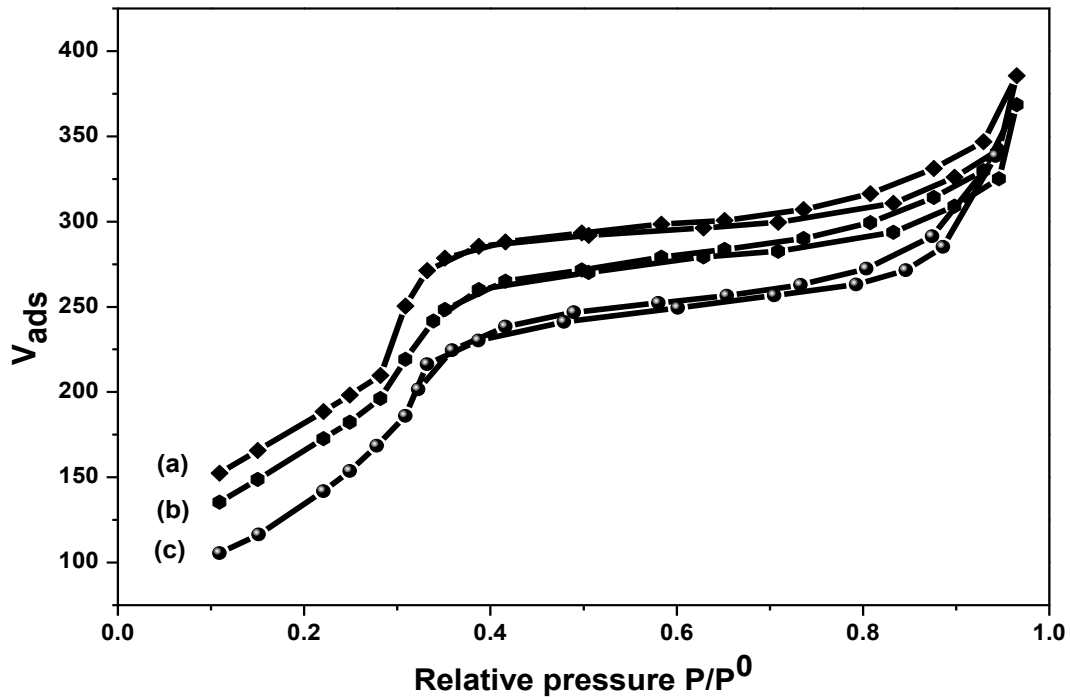


Fig 3: Adsorption –Desorption isotherms of nitrogen at  $-196^{\circ}\text{C}$  on pure MCM-41 calcined at  $550^{\circ}\text{C}$ .



**Fig 4:** Adsorption –Desorption isotherms of nitrogen at  $-196^{\circ}\text{C}$  on (a) 2%, (b) 8%, (c) 15%, (d) 25%, (e) 35% and (f) 45%  $\text{TiO}_2 / \text{MCM-41}$  calcined at  $550^{\circ}\text{C}$ .



**Fig 5:** Adsorption –Desorption isotherms of nitrogen at  $-196^{\circ}\text{C}$  on 25%  $\text{TiO}_2/\text{MCM-41}$  calcined at (a)  $450^{\circ}\text{C}$ , (b)  $550^{\circ}\text{C}$  and (c)  $650^{\circ}\text{C}$ .

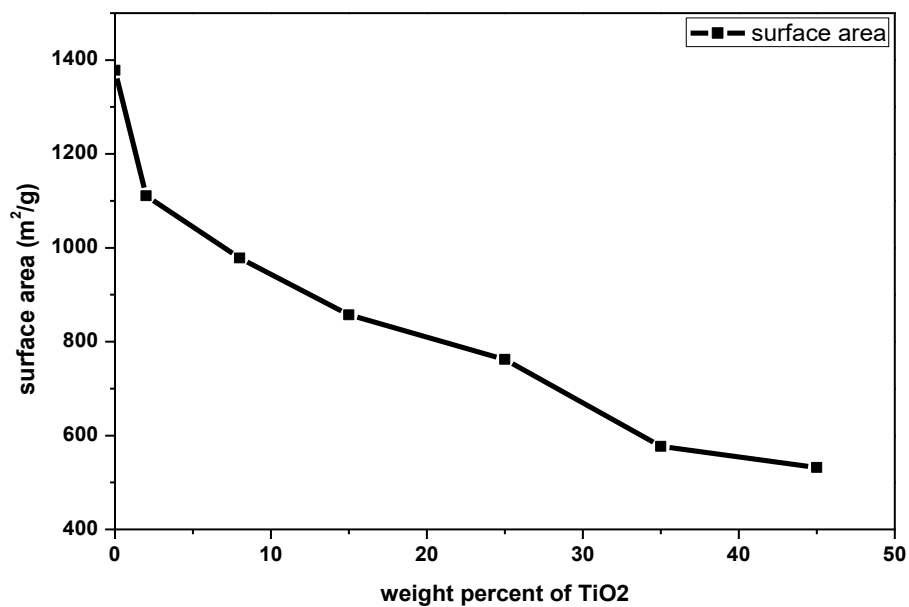


**Fig 6:** effect of weight content of TiO<sub>2</sub> on surface area.

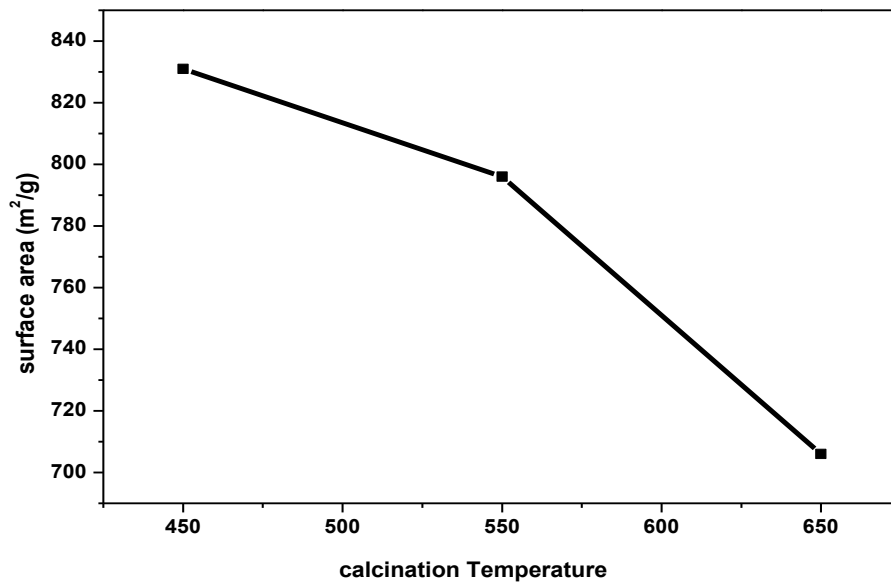


**Fig 7:** effect of calcination temperature on 25% TiO<sub>2</sub>/MCM-41 on surface area.

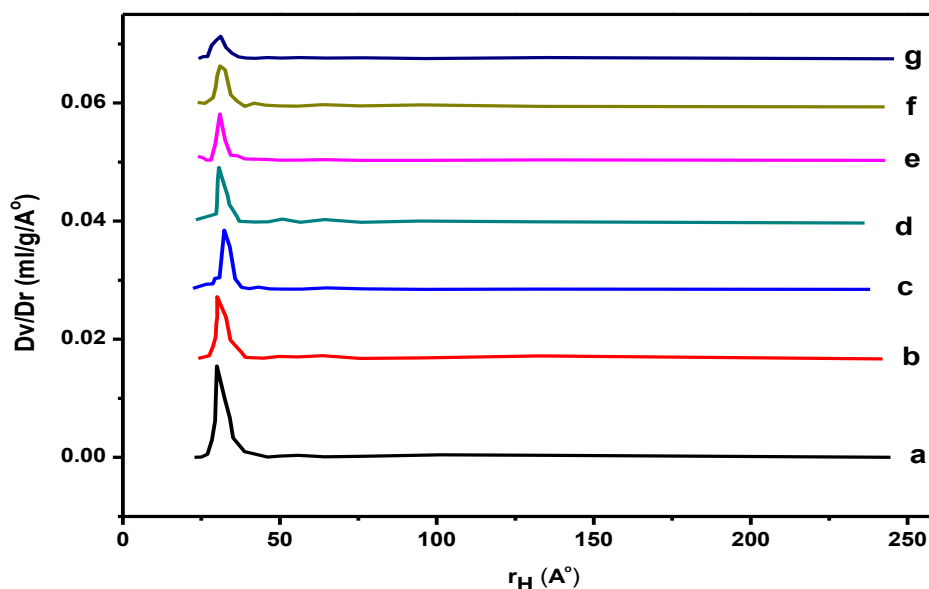


**Fig 8:** Pore volume distribution for (a) Pure MCM-41, (b) 2%, (c) 8%, (d) 15%, (e) 25%, (f) 35% and (g) 45% TiO<sub>2</sub>/MCM-41 calcined at 550°C.

**Table 2:** Surface characteristics of pure MCM-41 and TiO<sub>2</sub>/MCM-41.

adsorbents	$S_{BET}$ $m^2/g$	$S_a$ $m^2/g$	$C$	$V_T$ $ml/g$	$r^-$ $nm$
MCM-41 (550°C)	1378	1367	8.367	1.83	2.67
2% TM (550°C)	1111	1102	11.93	1.085	1.83
8% TM (550°C)	978	971	18.09	0.884	1.81
15% TM (550°C)	857	861	18.91	0.702	1.64
25% TM (550°C)	796	789	22.55	0.528	1.33
35% TM (550°C)	577	584	17.54	0.458	1.59
45% TM (550°C)	532	538	6.65	0.354	1.33
25% TM (450°C)	831	827	14.805	0.557	1.34
25% TM (550°C)	796	789	22.55	0.528	1.33
25% TM (650°C)	706	701	8.422	0.511	1.45

### 3.3. FT-IR spectra:

The frequencies of FTIR bands from pure MCM-41 and TiO<sub>2</sub>/MCM-41 observed in Fig 9 that shows the spectra of pure MCM-41 as well as 2, 8, 25, 45% TiO<sub>2</sub>/MCM-41 samples calcined at 550°C in the region of 400–4000 cm<sup>-1</sup>. A broad band around at 3460 cm<sup>-1</sup> can be observed in all samples, which is mainly caused by the O–H stretching vibration of the adsorbed water molecules or Si–O–H, while bending vibration mode of water is signified to the band recorded at 1630 cm<sup>-1</sup>. The strong vibration band at 1069 cm<sup>-1</sup> in pure MCM-41 assigned to asymmetric stretching of Si–O–Si shifted to 1089 cm<sup>-1</sup> in TiO<sub>2</sub>/MCM-41 samples. Wave number for asymmetric stretching of Si–O–Si has shifted from lower to higher value when titanium was loaded into MCM-41. A peak at 954 cm<sup>-1</sup> in TiO<sub>2</sub>/MCM-41 sample is more intense as compared to the peak present in pure MCM-41. It is reported that the peak around 910–960 cm<sup>-1</sup> is due to the Si–O stretching vibration of a polarized Si–O<sup>δ-</sup>–Ti<sup>δ+</sup> bond (Li et al., 2005; Wang et al., 2006; Zhang et al., 2005). In our samples peak has been observed at 954 cm<sup>-1</sup> which is at slightly lower wave number. This however may be due to Si–O–Ti vibration. The peak at 960 cm<sup>-1</sup> in pure MCM-41 is more intense and can be attributed to the silanol Si–OH vibration. It is observed that peak at 960 cm<sup>-1</sup> in MCM-41 is narrow and more intense due to free vibration of Si–OH bond as compared to TiO<sub>2</sub>/MCM-41 sample. This supports that, the TiO<sub>2</sub> nanoparticles are bonded with silica by Si–O–Ti bond. Two more bands at ca 800 and 458

$\text{cm}^{-1}$  are ascribed to symmetric stretching vibration and bending vibration of rocking mode of Si–O–Si, respectively. The anatase and rutile phases of  $\text{TiO}_2$  exhibit bands in the  $650\text{--}850\text{ cm}^{-1}$  and  $600\text{--}850\text{ cm}^{-1}$  regions, respectively (Sudarsanam and Reddy, 2013). In the present work, XRD characterization indicated that the surfaces of the adsorbents were only anatase phase  $\text{TiO}_2$ . In agreement with the XRD results, the IR spectra showed a band at  $679\text{ cm}^{-1}$ , which suggests that anatase phase  $\text{TiO}_2$  is present on the surface of the MCM-41. Fig 10 shows the effect of calcination temperature on the IR spectra of 25%  $\text{TiO}_2/\text{MCM-41}$ . It can be seen that no effect can be observed with increase the calcination temperature to  $550^\circ\text{C}$  and  $650^\circ\text{C}$ . This implies also that the  $\text{TiO}_2$  particles are chemically adsorbed on the surface of MCM-41.

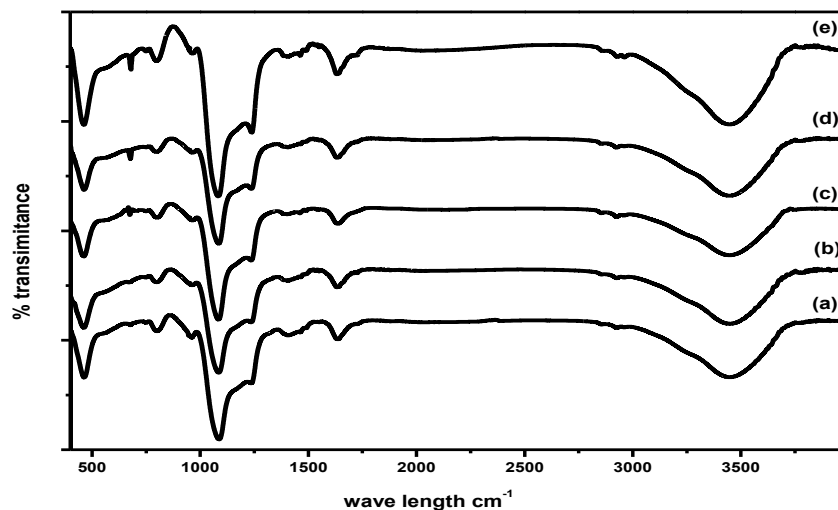


**Fig 9:** FTIR spectra of (a) MCM-41, (b) 2%, (c) 8%, (d) 25% and (e) 45%  $\text{TiO}_2/\text{MCM-41}$  calcined at  $550^\circ\text{C}$ .

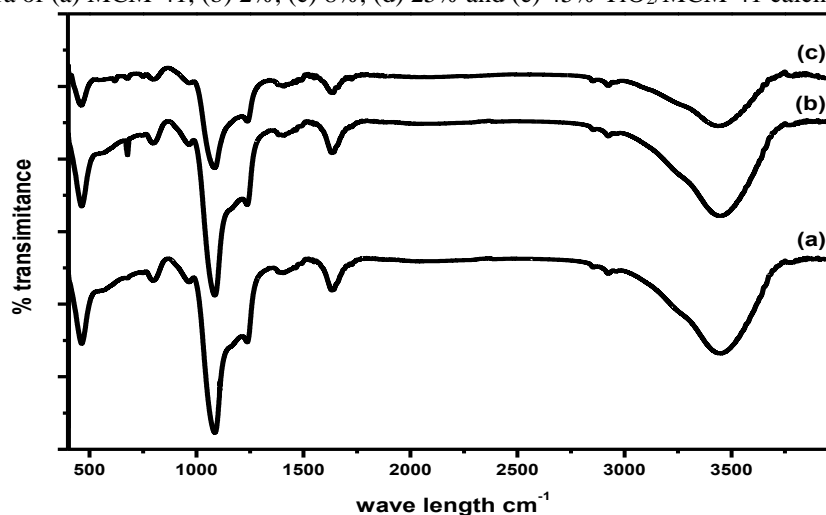


**Fig 10:** FTIR spectra of 25%  $\text{TiO}_2/\text{MCM-41}$  calcined at (a)  $450^\circ\text{C}$ , (b)  $550^\circ\text{C}$  and (c)  $650^\circ\text{C}$ .

### 3.4. Transmission electron Microscopy (TEM image)

To elucidate the pore structure of MCM-41 transmission electron microscopy is usually used. TEM images of pure MCM-41 display an order structure with uniform mesoporous arranges into hexagonal, honey comb-like lattice as shown in Fig 11. MCM-41 exhibits regular pore with size nearly equal 3 nm. TEM images of pure MCM-41 show the existence of nanosized (elongated) spherical particles and hexagonal arrays. Morphology structure and uniform dispersion of obtained  $\text{TiO}_2/\text{MCM-41}$  samples are clearly revealed by TEM image which can be distinguished as dark dots. Fig 11 shows TEM images of 2, 25 and 45 wt%  $\text{TiO}_2/\text{MCM-41}$  samples calcined at  $550^\circ\text{C}$ , which exhibit ordered hexagonal array of mesoporous structures. As shown in Fig 11, the ordered mesoporous structure of MCM-41 samples is kept unaffected in the presence of  $\text{TiO}_2$  (Hui and Chao, 2006; Ma et al., 2013). Darker spots appear in the TEM images of the MCM-41 which could be attributed to some  $\text{TiO}_2$  within the pores and/or on the surface of the MCM-41 crystals. Also, the number of dark spots increases with increases  $\text{TiO}_2$  content. The crystallite sizes which calculate from x- ray diffraction patterns have nearly the same values as

observed at TEM image. Table 1 shows the variation of crystal size values which are obtained from TEM images and x-ray diffraction patterns for 2, 25 and 45 wt.% of TiO<sub>2</sub>/MCM-41.

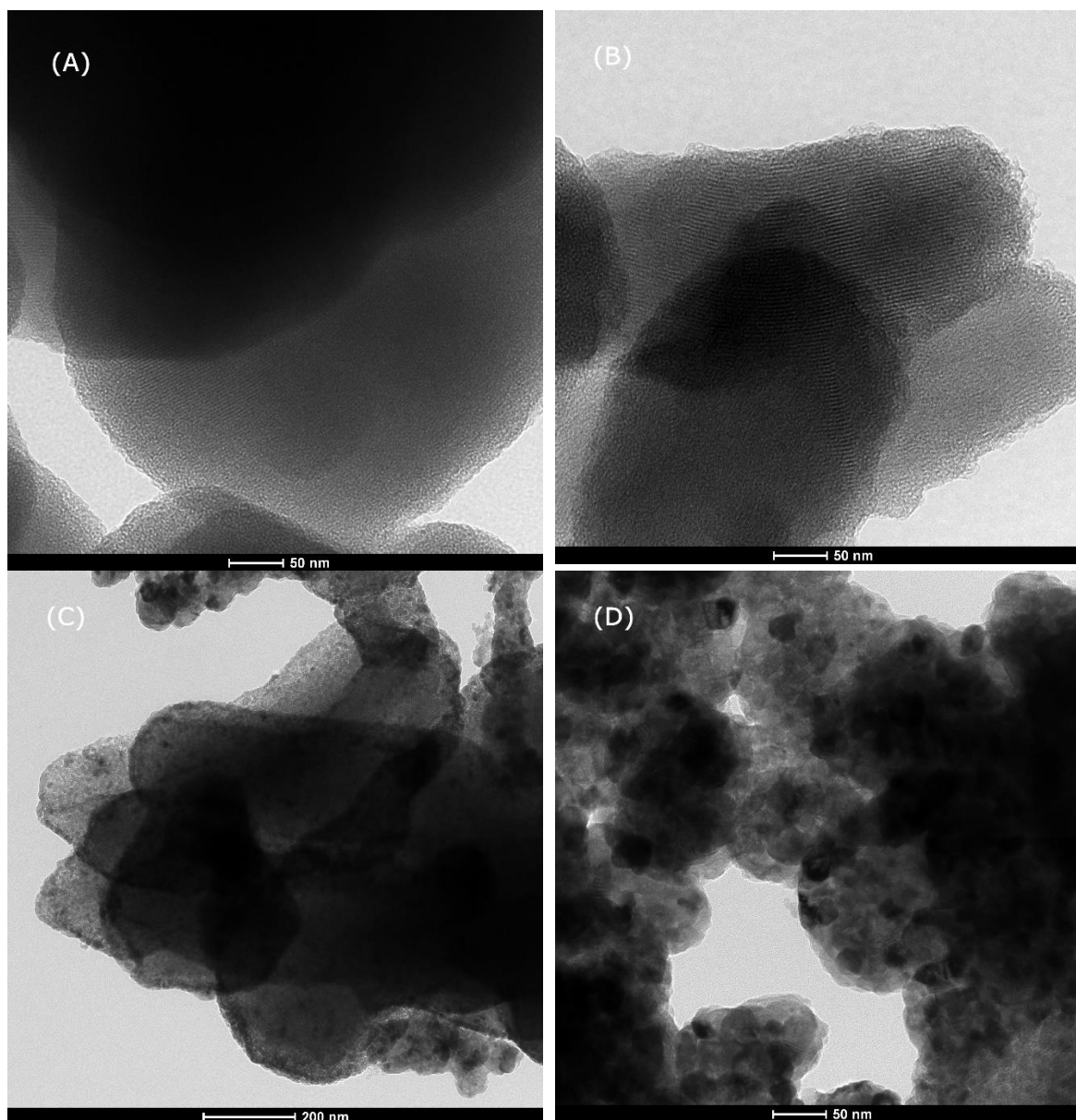


**Fig. 11:** TEM images of (A) pure MCM-41, (B) 2% TiO<sub>2</sub> / MCM-41, (C) 25% TiO<sub>2</sub> / MCM-41 and (D) 45% TiO<sub>2</sub> / MCM-41 calcined at 550°C.

### 3.5. adsorption activity

Dyes are widely used in industries such as textiles, leather, printing, food, and plastics, etc. The removal of dyes from industrial wastewaters is a major problem. Conventional methods for the removal of dyes from wastewater include adsorption onto solid substrates, chemical coagulation, oxidation, filtration and biological treatment. Adsorption is one of the effective separation techniques to remove dilute pollutants as well as offering the potential for regeneration, recovery and recycling of the adsorbing material.

#### 3.5.1. The effect of pH:

Fig 12 depicts  $q_e$  versus pH for 25% TiO<sub>2</sub>/MCM-41 calcined at 550°C. Evidently, successive increase of  $q_e$  is shown with the increase of pH from 2 to 10. Fig 12 shows that pH at 8-10 is the best point for adsorption of MB.

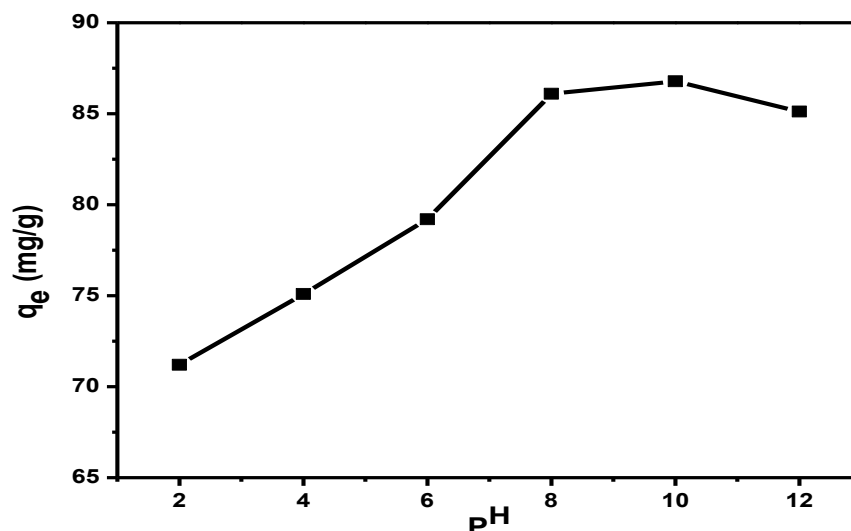


**Fig 12:** Effect of pH on adsorption of methylene blue by 25% TiO<sub>2</sub>/MCM-41 calcined at 550°C.

### 3.5.2 Equilibrium Adsorption isotherm:

The analysis and design of the adsorption process requires the relevant adsorption equilibrium, which is the most important piece of information in understanding an adsorption process. The isotherm data were obtained by plotting the amount of dye adsorbed on the solid (mg/g) against the remaining concentration of dye in the solution (mg/L), generally called equilibrium concentration as shown in Fig 13.

Langmuir adsorption isotherm model can be written as

$$\frac{1}{q_e} = \frac{1}{K_L q_m} + \frac{1}{C_e}$$

Where  $q_e$  is the equilibrium dye concentration on the adsorbent (mg /g),  $C_e$  the equilibrium dye concentration in the solution (mg /L),  $q_{max}$  the monolayer adsorption capacity of the adsorbent (mg /g), and  $K_L$  is the Langmuir adsorption constant (L/mg) related to the heat of adsorption.

The linear form of Langmuir isotherm can be represented as:

$$\frac{C_e}{q_e} = \frac{1}{b q_m} + \frac{1}{q_m} C_e$$

A straight line of slope =  $\frac{1}{q_m}$  and intercept =  $\frac{1}{b q_m}$  is obtained when  $C_e / q_e$  is plotted against  $C_e$  in Fig 14.

One of the essential characteristics of the Langmuir isotherm can be expressed by a separation factor,  $R_L$ ; which can be calculated from:

$$R_L = \frac{1}{1 + b C_0}$$

Where  $C_0$  is the highest initial solute concentration and the  $R_L$  value implies whether the adsorption is unfavorable ( $R_L > 1$ ), linear ( $R_L = 1$ ), favorable ( $0 < R_L < 1$ ), or irreversible ( $R_L = 0$ ). It was observed that all the  $R_L$  values obtained were between 0 and 1, showing that the adsorption of MB on TiO<sub>2</sub> / MCM-41 samples were favorable.

Freundlich isotherm is an adsorption model for a single solute system. Freundlich model is based on an empirical equation of the distribution of solute between the solid phase and aqueous phase at equilibrium. It is not restricted to the formation of a monolayer in comparison with Langmuir theory. The well-known logarithmic form of Freundlich is given by the following equation:

$$\log q_e = \frac{1}{n} \log C_e + \log K_F$$

Where  $K_F$  and  $n$  are Freundlich constants related to adsorption capacity and adsorption intensity, respectively. In general  $n > 1$  illustrates that adsorbate is favorably adsorbed on the adsorbent whereas  $n < 1$  demonstrates the adsorption process is chemical in nature. The plot of  $\log(q_e)$  versus  $\log(C_e)$  gave a straight line with slope of  $1/n$  and intercept of  $\ln K_F$ . Fig 15 shows satisfactory linear plots indicating the fitting of the MB adsorption data to the Freundlich equation. Also, high values of  $R^2$ , i.e. between 0.8968 and 0.9331 were obtained. The Freundlich constants as determined from the linear Freundlich plots, together with corresponding values of  $R^2$  are listed in Table 3. The values found for  $n$  were between 3.41 and 4.1, which prove that the adsorption is favorable and process is physical in nature. Also, the values of  $q_{max}$  and Langmuir constants determined by the application of the Langmuir model are included in table 3.

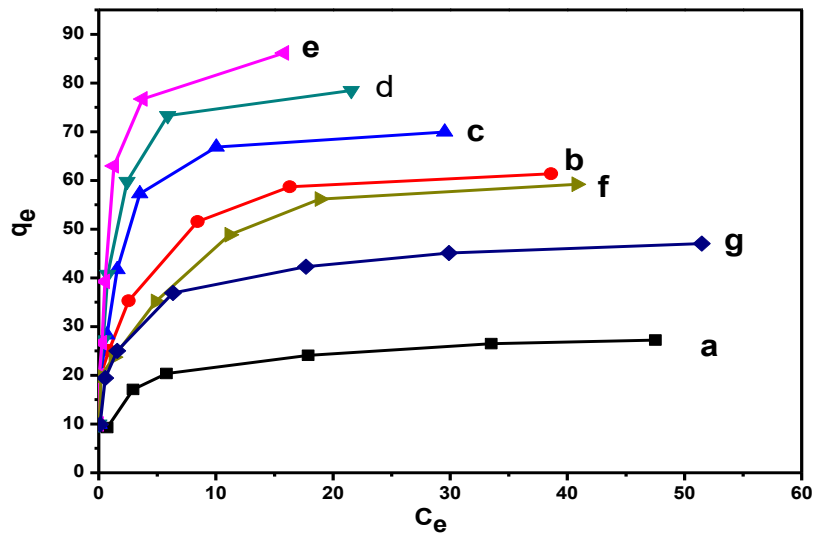


**Fig 13:** Equilibrium adsorption isotherm of methylene blue onto (a) pure MCM-41, (b) 2%, (c) 8%, (d) 15%, (e) 25%, (f) 35% and (g) 45% TiO<sub>2</sub>/MCM-41.

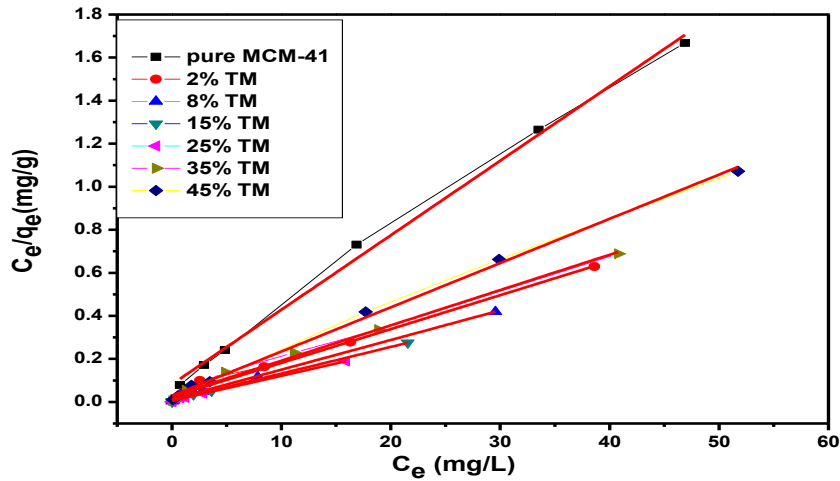


**Fig 14:** Linear form of Langmuir isotherm for methylene blue onto pure MCM-41 and different weight content of TiO<sub>2</sub> loaded on MCM-41.

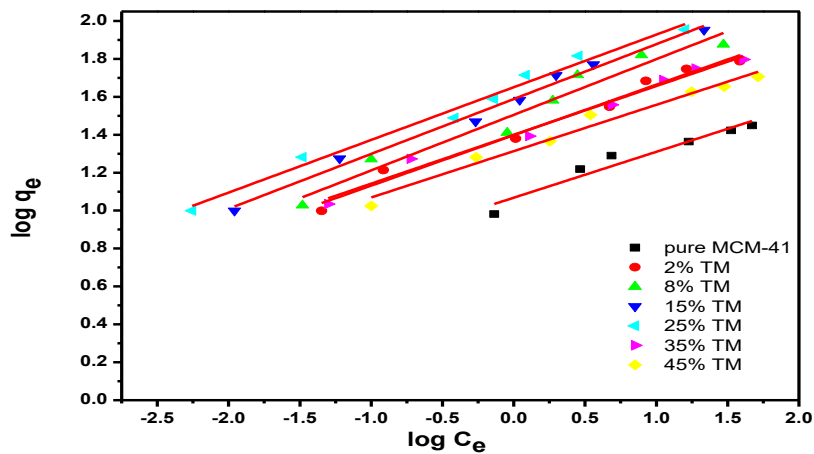


**Fig 15:** Linear form of Freundlich isotherm for methylene blue onto pure MCM-41 and different weight of TiO<sub>2</sub> loaded on MCM-41.

**Table 3;** Adsorption isotherm parameters for MB on pure MCM-41 and TiO<sub>2</sub>/MCM-41.

Sample	Langmuir isotherm			Freundlich isotherm			
	q <sub>max</sub> (mg/g)	K <sub>L</sub> (L/mg)	R <sup>2</sup>	R <sub>L</sub>	K <sub>F</sub> (mg/g)	n	R <sup>2</sup>
Pure MCM-41	28.89	0.4221	0.99586	0.023	11.71	4.098	0.89686
2% (TM)	64.35	0.5072	0.97781	0.019	26.3	3.981	0.93312
8% (TM)	72.57	1.116	0.99572	0.0089	31.92	3.413	0.89839
15% (TM)	80.71	1.5334	0.99597	0.00648	39.01	3.490	0.91737
25% (TM)	86.66	1.936	0.99562	0.00514	44.61	3.597	0.92077
35% (TM)	60.98	0.592	0.9921	0.017	24.53	3.876	0.95762
45% (TM)	48.64	0.4221	0.99732	0.023	20.62	4.048	0.92487

### 3.5.3. Dynamic adsorption of methylene blue:

Kinetic study is one of the most important methods to evaluate the efficiency of adsorption. It describes the rate of adsorbate uptake onto TiO<sub>2</sub>/MCM-41 samples and the equilibrium time. The effects of contact time on the adsorption of MB on different samples are shown in Fig 16.

The amount of dye adsorbed at time t, q<sub>t</sub> (mg/g) was calculated using the following equation:

$$q_t = \frac{(C_0 - C_t)V}{M}$$

Where C<sub>0</sub> and C<sub>t</sub> (mg/L) are the initial concentration and the concentration of the dye adsorption solution at time t, V is the volume of solution in (L) and M is the mass of adsorbent in (g).

Fig 16 shows an increase in adsorption capacity with time for all investigated samples. However, the adsorption was faster at the initial stages but progressively slowed down with time until equilibrium was finally attained. This is attributed to the large number of vacant sites available for adsorption at the initial than the later stages.

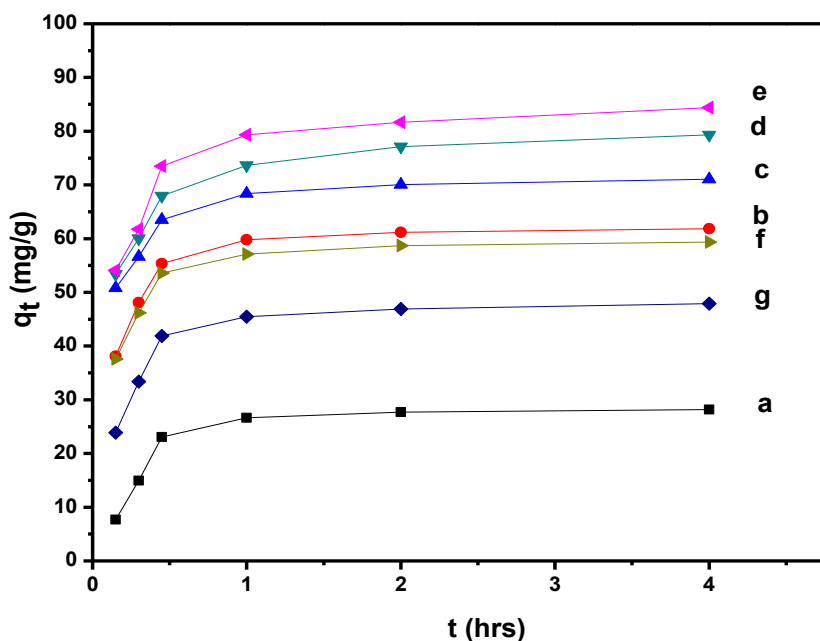


**Fig 16:** Kinetic adsorption curves of MB over (a) pure MCM-41, (b) 2%, (c) 8%, (d) 15%, (e) 25%, (f) 35% and (g) 45% TiO<sub>2</sub>/MCM-41.

The kinetic models used in order to investigate the mechanism of adsorption, were the pseudo first order and the pseudo- second order kinetic models and the intraparticle diffusion models. The form of the pseudo- first order model of adsorption can be expressed in the following equation:

$$\log(q_e - q_t) = \log q_e - \frac{k_1}{2.303} t$$

Where  $q_e$  and  $q_t$  (mg/g) are the amounts of dye adsorbed at equilibrium and at time  $t$ , respectively and  $k_1$ , is the equilibrium constant ( $\text{min}^{-1}$ ). Fig 17 shows the application of linear pseudo first order model to the kinetic adsorption.

While the form of the pseudo- Second order reaction equation may be written as

$$\frac{t}{q_t} = \frac{1}{k_2 q_e^2} + \frac{1}{q_e} t.$$

Where  $K_2$  is the pseudo-second-rate constant ( $\text{mg/g.min}$ ). Fig 18 shows the application of linear pseudo second order model to the kinetic adsorption. The kinetic adsorption constants as determined by the application of the pseudo first order and the pseudo- second order kinetic models are listed in table 4.

Evidently the application of the pseudo first order model to the kinetic adsorption curve of MB gave  $q_e$  values significantly lower than the corresponding experimental ones. Also, the values of the correlation coefficient  $R^2$  were relatively low compared with those obtained when the pseudo second order model was considered. These suggested that the pseudo-second-order adsorption mechanism was predominant referring that adsorption process is controlled by chemisorption which involves valency forces through sharing or exchange of electron between the solvent and the adsorbate (Ahmad and Rahman, 2011). Since neither the pseudo-first-order nor the second-order model can clarify the diffusion mechanism, the kinetic results were further analyzed by the intraparticle diffusion mode to clarify the diffusion mechanism.

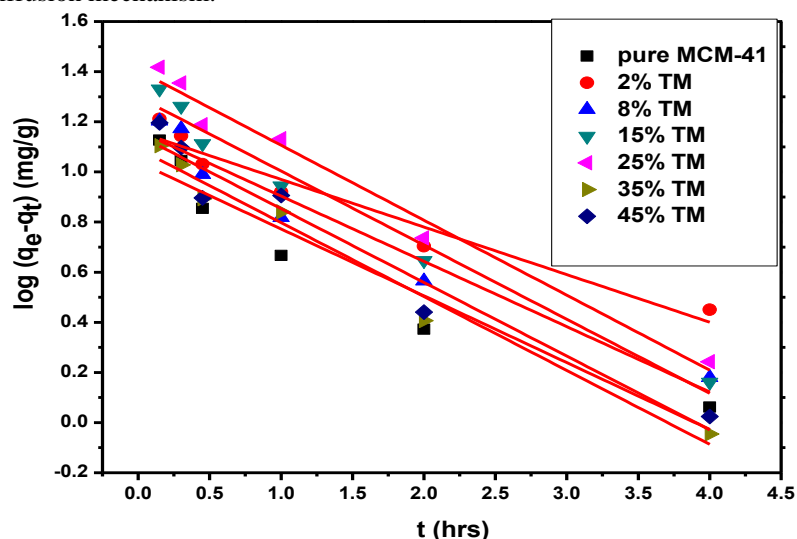


Fig 17: Pseudo first order kinetic model for adsorption of MB onto pure MCM-41 and different weight content of  $\text{TiO}_2$  loaded on MCM-41.

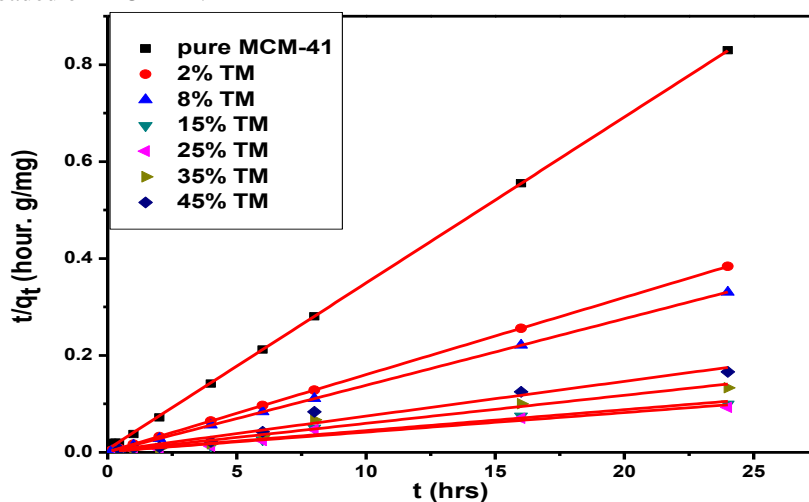


Fig 18: Pseudo second order kinetic model for adsorption of MB onto pure MCM-41 and different weight content of  $\text{TiO}_2$  loaded on MCM-41.

**Table 4:** kinetic model parameters (pseudo 1<sup>st</sup> order and pseudo 2<sup>nd</sup> order) for adsorption of methylene blue onto investigated adsorbents.

sample	$q_{e(\text{Exp})}$ (mg/g)	Pseudo-first-order-kinetic- model			Pseudo-second-order-kinetic- model		
		$q_{e1}$ (mg/g)	$K_1$ (1/hr)	$R^2$	$q_{e2}$ (mg/g)	$K_2$ (g/mg.hr)	$R^2$
MCM-41	28.89	10.94	0.614	0.90305	29.19	0.1739	0.9998
2% TM	64.35	14.45	0.437	0.93719	62.77	0.2350	0.9999
8% TM	72.57	16.14	0.599	0.94576	72.78	0.1748	0.9998
15% TM	80.71	19.91	0.681	0.97359	80.91	0.1441	0.9997
25% TM	86.66	25.44	0.689	0.97681	89.18	0.1115	0.9999
35% TM	60.98	12.38	0.679	0.97303	60.50	0.2296	0.9995
45% TM	48.64	14.04	0.675	0.94463	48.99	0.1819	0.9998

### 3.5.4. Adsorption mechanism:

The intraparticle diffusion model was first proposed by Weber and Morris (Kumar et al., 2010). Who concluded that the uptake was proportional to the square root of the contact time during the course of adsorption

$$q_t = K_d t^{0.5} + C$$

Where  $K_d$  is the rate constant of the intraparticle transport [mg/g.h<sup>0.5</sup>]. The value of  $K_d$  is obtained from the slope of the straight line, where  $C$  is the intercept. The parameters  $K_d$ ,  $C$  and  $R^2$  are listed in table 5. As shown in Fig. 19, the dual nature of the curves was obtained due to the varying extent of sorption in the initial and final stages of the experiment. The first sharper portion was the external surface adsorption. The second portion was the gradual adsorption where the intraparticle diffusion was rate limiting. If the lines don't pass through the origin point, therefore Intraparticle diffusion is not the only rate limiting step and indicates the effect of film diffusion (boundary layer diffusion) on adsorption of dyes. In order to predict the real slow step involved, the kinetic data were further analyzed using the Boyd kinetic expression. This kinetic expression predicts the actual slowest step involved in the adsorption process.

Boyd kinetic equation (El-Khaiary and Malash, 2011) was applied, which is represented as:

$$F(t) = 1 - \frac{6}{\pi^2} \sum_{n=1}^{\infty} \frac{1}{n^2} \exp(-n^2 B t)$$

Where  $f$  is the fractional attainment of equilibrium at different times ( $t$ ), and  $B(t)$  is a mathematical function of  $F$ .

$$F = \frac{q_t}{q_e}$$

Where  $q_t$  and  $q_e$  is the amount adsorbed at time ( $t$ ) and equilibrium respectively. Reichenberg (Reichenberg, 1953) managed to obtain the following approximations:

$$B(t) = -0.4977 - \ln(1 - F) \quad \text{when } F > 0.85$$

$$B(t) = (\sqrt{\pi} - \sqrt{\pi - \left(\frac{\pi^2 F(t)}{3}\right)})^2 \quad \text{when } F < 0.85$$

The plot of  $B(t)$  against time  $t$  can be employed to test the linearity of the experimental values. If the plots are linear and pass-through origin, then the slowest (rate controlling) step in the adsorption process is the internal diffusion, and vice versa. From Fig 20, it was observed that the plots are linear but do not pass through the origin suggesting that the adsorption process is controlled by film diffusion.

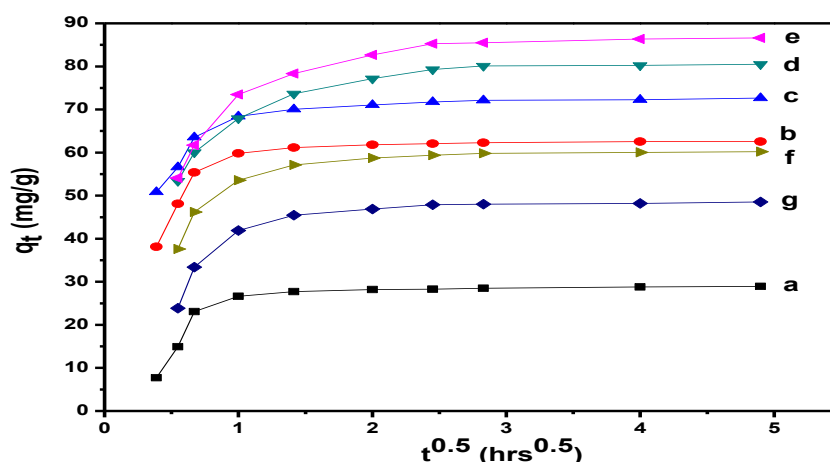


**Fig 19:** Intraparticle diffusion plot for adsorption of methylene blue onto (a) pure McM-41, (b) 2%, (c) 8%, (d) 15%, (e) 25%, (f) 35% and (g) 45% TiO<sub>2</sub>/McM-41.

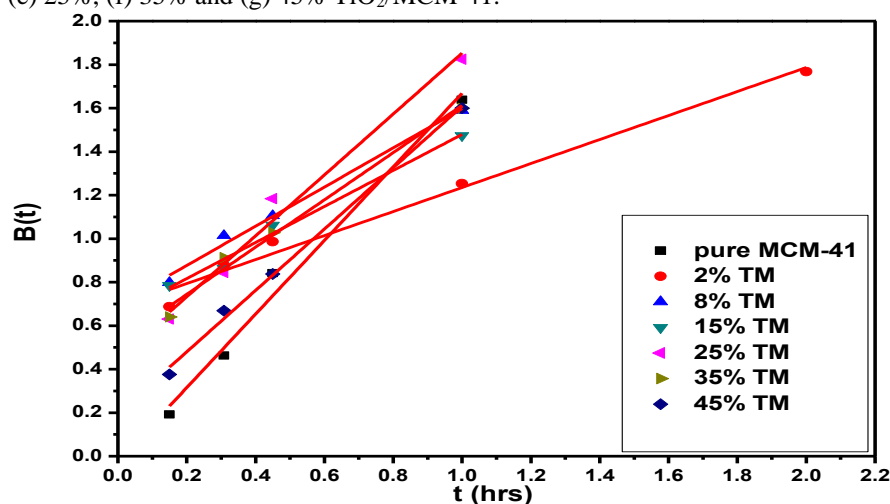


**Fig 20:** Boyd plot for adsorption of MB onto pure MCM-41 and different weight content of TiO<sub>2</sub> loaded on MCM-41.

**Table 5:** Intra-particle diffusion and Boyd plot parameters for adsorption of MB onto investigated adsorbents:

Samples	Intraparticle diffusion			Boyd plot	
	$K_d$ (mg/g.h <sup>0.5</sup> )	C (mg/gm)	R <sup>2</sup>	Intercept	R <sup>2</sup>
MCM-41	0.2668	27.68	0.9492	-0.0232	0.9819
2% TM	0.2434	61.46	0.8285	0.6831	0.9802
8% TM	0.4567	70.49	0.8573	0.6967	0.9874
15% TM	0.3637	78.97	0.9194	0.6533	0.9851
25% TM	0.5335	84.39	0.8894	0.5201	0.9907
35% TM	0.2755	59.06	0.8292	0.5312	0.9802
45% TM	0.3216	47.25	0.9904	0.2031	0.9904

#### 4. Conclusion

In this study, Solid acid material of MCM-41 prepared by sol-gel method followed by incorporation of TiO<sub>2</sub> within the mesochannels through a simple and effective impregnation method. Structure characterization of the prepared adsorbents and phase changes were determined using X-ray, TEM and FT-IR techniques, the results

have shown that presence of sharp peak at  $2\theta$  (2.4) which implies the hexagonal pore structure of all samples. For  $\text{TiO}_2$  / MCM-41 adsorbent, the addition of  $\text{TiO}_2$  stabilizes the tetragonal anatase phase of  $\text{TiO}_2$ . As  $\text{TiO}_2$  loading increase, characteristic peaks for anatase phase are formed. TEM images of pure MCM-41 show the existence of nanosized (elongated) spherical particles and hexagonal arrays. Darker spots appear in the TEM attributed to some  $\text{TiO}_2$  within the pores and/or on the surface of the MCM-41 crystals that increases with increases  $\text{TiO}_2$  content. It was found that the surface area of MCM-41 determined by BET method was found to be  $1378 \text{ m}^2/\text{g}$ . The surface area values decrease on increasing the  $\text{TiO}_2$  content due to the deposition of  $\text{TiO}_2$  particles on the surface and pores of MCM-41. addition of  $\text{TiO}_2$  to MCM-41 was accompanied by gradual increases in acid strength up to 25wt%  $\text{TiO}_2$ . This may be due to the good dispersion of  $\text{TiO}_2$  on the surface of MCM-41 which leads to the generation of acid sites.

### Disclosure

This research did not receive any specific grant from funding agencies in the public, commercial or not-for-profit sectors. There is no Conflict of Interest

### References

- Ahmad, M.A., Rahman, N.K., 2011. Equilibrium, kinetics and thermodynamic of Remazol Brilliant Orange 3R dye adsorption on coffee husk-based activated carbon. *Chem. Eng. J.* 170, 154–161.
- Ahmed, A.I., El-Hakam, S.A., Khder, A.S., El-Yazeed, W.S.A., 2013. Nanostructure sulfated tin oxide as an efficient catalyst for the preparation of 7-hydroxy-4-methyl coumarin by Pechmann condensation reaction. *J. Mol. Catal. A Chem.* 366, 99–108.
- Alshorifi, F.T., Alswat, A.A., Mannaa, M.A., Alotaibi, M.T., El-Bahy, S.M., Salama, R.S., 2021. Facile and Green Synthesis of Silver Quantum Dots Immobilized onto a Polymeric CTS–PEO Blend for the Photocatalytic Degradation of p-Nitrophenol. *ACS Omega* 6, 30432–30441.
- Aronson, B.J., Blanford, C.F., Stein, A., 1997. Solution-phase grafting of titanium dioxide onto the pore surface of mesoporous silicates: synthesis and structural characterization. *Chem. Mater.* 9, 2842–2851.
- Bandyopadhyay, M., Birkner, A., Van den Berg, M.W.E., Klementiev, K. V, Schmidt, W., Grünert, W., Gies, H., 2005. Synthesis and characterization of mesoporous MCM-48 containing  $\text{TiO}_2$  nanoparticles. *Chem. Mater.* 17, 3820–3829.
- Cañizares, P., Martínez, F., Jiménez, C., Lobato, J., Rodrigo, M.A., 2006. Coagulation and electrocoagulation of wastes polluted with dyes. *Environ. Sci. Technol.* 40, 6418–6424.
- Chen, X., Lam, K.F., Zhang, Q., Pan, B., Arruebo, M., Yeung, K.L., 2009. Synthesis of highly selective magnetic mesoporous adsorbent. *J. Phys. Chem. C* 113, 9804–9813.
- Crini, G., 2006. Non-conventional low-cost adsorbents for dye removal: a review. *Bioresour. Technol.* 97, 1061–1085.
- Do, Y.-J., Kim, J.-H., Park, J.-H., Park, S.-S., Hong, S.-S., Suh, C.-S., Lee, G.-D., 2005. Photocatalytic decomposition of 4-nitrophenol on Ti-containing MCM-41. *Catal. today* 101, 299–305.
- Eimer, G.A., Casuscelli, S.G., Chanquia, C.M., Elías, V., Crivello, M.E., Herrero, E.R., 2008. The influence of Ti-loading on the acid behavior and on the catalytic efficiency of mesoporous Ti-MCM-41 molecular sieves. *Catal. Today* 133, 639–646.
- El-Hakam, S.A., AlShorifi, F.T., Salama, R.S., Gamal, S., El-Yazeed, W.S.A., Ibrahim, A.A., Ahmed, A.I., 2022. Application of nanostructured mesoporous silica/bismuth vanadate composite catalysts for the degradation of methylene blue and brilliant green. *J. Mater. Res. Technol.* 18, 1963–1976.
- El-Hakam, S.A., Ibrahim, A.A., Elatwy, L.A., El-Yazeed, W.S.A., Salama, R.S., Abou El-Reash, Y.G., Ahmed, A.I., 2021. Greener route for the removal of toxic heavy metals and synthesis of 14-aryl-14H dibenzo [a, j] xanthene using a novel and efficient Ag-Mg bimetallic MOF as a recyclable heterogeneous nanocatalyst. *J. Taiwan Inst. Chem. Eng.*
- El-Hakam, S.A., Samra, S.E., El-Dafrawy, S.M., Ibrahim, A.A., Salama, R.S., 2013a. Surface Acidity and Catalytic Activity of Sulfated Titania Supported on Mesoporous MCM-41. *Int. J. Mod. Chem. Int. J. Mod. Chem. J.* homepage [www.ModernScientificPress.com/Journals/IJMChem.aspx](http://www.ModernScientificPress.com/Journals/IJMChem.aspx) 5, 55–70.
- El-Hakam, S.A., Samra, S.E., El-Dafrawy, S.M., Ibrahim, A.A., Salama, R.S., 2013b. Surface acidity and catalytic activity of sulfated titania supported on mesoporous MCM-41. *Int. J. Mod. Chem* 5, 55–70.
- El-Hakam, S.A., Samra, S.E., El-Dafrawy, S.M., Ibrahim, A.A., Salama, R.S., Ahmed, A.I., 2018. Synthesis of sulfamic acid supported on Cr-MIL-101 as a heterogeneous acid catalyst and efficient adsorbent for methyl

- orange dye. RSC Adv. 8, 20517–20533. <https://doi.org/10.1039/c8ra02941e>
- El-Khaiary, M.I., Malash, G.F., 2011. Common data analysis errors in batch adsorption studies. *Hydrometallurgy* 105, 314–320.
- El-Sheekh, M.M., Ghariieb, M.M., Abou-El-Souod, G.W., 2009. Biodegradation of dyes by some green algae and cyanobacteria. *Int. Biodeterior. Biodegradation* 63, 699–704.
- El-Yazeed, W.S.A., El-Hakam, S.A., Salama, R.S., Ibrahim, A.A., Ahmed, A.I., 2022. Ag-PMA supported on MCM-41: Surface Acidity and Catalytic Activity. *J. Sol-Gel Sci. Technol.* 102, 387–399.
- Freundlich, H., 1907. Über die adsorption in lösungen. *Zeitschrift für Phys. Chemie* 57, 385–470.
- Hsien, Y.-H., Chang, C.-F., Chen, Y.-H., Cheng, S., 2001. Photodegradation of aromatic pollutants in water over TiO<sub>2</sub> supported on molecular sieves. *Appl. Catal. B Environ.* 31, 241–249.
- Hui, K.S., Chao, C.Y.H., 2006. Synthesis of MCM-41 from coal fly ash by a green approach: Influence of synthesis pH. *J. Hazard. Mater.* 137, 1135–1148.
- Ibrahim, A.A., Salama, R.S., El-hakam, S.A., Khder, A.S., Ahmed, A.I., 2021. Synthesis of 12-tungstophosphoric acid supported on Zr / MCM-41 composite with excellent heterogeneous catalyst and promising adsorbent of methylene blue. *Colloids Surfaces A Physicochem. Eng. Asp.* 631, 127753.
- Jermly, B.R., Pandurangan, A., 2008. Synthesis of geminal diacetates (acylals) using heterogeneous H<sub>3</sub>PW<sub>12</sub>O<sub>40</sub> supported MCM-41 molecular sieves. *Catal. Commun.* 9, 577–583.
- Kumar, R.P., Varanasi, S., Purushothaman, V., 2010. Investigation of the biosorption mechanisms of Methylene blue onto press mud through kinetic modeling analysis. *Indian J. Sci. Technol.* 3, 44–47.
- Lassaletta, G., Gonzalez-Elipse, A.R., Justo, A., Fernandez, A., Ager, F.J., Respaldiza, M.A., Soares, J.C., Da Silva, M.F., 1996. Thermal and photochemical methods for the preparation of thin films of cermet materials. *J. Mater. Sci.* 31, 2325–2332.
- Li, Z., Hou, B., Xu, Y., Wu, D., Sun, Y., 2005. Hydrothermal synthesis, characterization, and photocatalytic performance of silica-modified titanium dioxide nanoparticles. *J. Colloid Interface Sci.* 288, 149–154.
- Ma, L., Ji, J., Yu, F., Ai, N., Jiang, H., 2013. Post-synthesis of TiO<sub>2</sub>/MCM-41 from aqueous TiCl<sub>4</sub> solution: Structure characteristics and epoxy catalytic activity. *Microporous Mesoporous Mater.* 165, 6–13.
- Mannaa, M.A., Altass, H.M., Salama, R.S., 2021a. MCM-41 grafted with citric acid: The role of carboxylic groups in enhancing the synthesis of xanthenes and removal of heavy metal ions. *Environ. Nanotechnology, Monit. Manag.* 15, 100410.
- Mannaa, M.A., Qasim, K.F., Alshorifi, F.T., El-Bahy, S.M., Salama, R.S., 2021b. Role of NiO Nanoparticles in Enhancing Structure Properties of TiO<sub>2</sub> and Its Applications in Photodegradation and Hydrogen Evolution. *ACS Omega* 6, 30386–30400.
- Parala, H., Winkler, H., Kolbe, M., Wohlfart, A., Fischer, R.A., Schmechel, R., von Seggern, H., 2000. Confinement of CdSe nanoparticles inside MCM-41. *Adv. Mater.* 12, 1050–1055.
- Radwan, N.R.E., El-Sharkawy, E.A., Youssef, A.M., 2005. Influence of gold and manganese as promoters on surface and catalytic performance of Fe<sub>2</sub>O<sub>3</sub>/Al<sub>2</sub>O<sub>3</sub> system. *Appl. Catal. A Gen.* 281, 93–106.
- Reichenberg, D., 1953. Properties of ion-exchange resins in relation to their structure. III. Kinetics of exchange. *J. Am. Chem. Soc.* 75, 589–597.
- Salama, R.S., 2019. Synthesis, characterization and Catalytic activities of sulfuric acid loaded on Copper metal organic frameworks (Cu-BDC). *Delta Univ. Sci. J.* 2, 2.
- Salama, Reda S, El-Bahy, S.M., Mannaa, M.A., 2021. Sulfamic acid supported on mesoporous MCM-41 as a novel, efficient and reusable heterogeneous solid acid catalyst for synthesis of xanthene, dihydropyrimidinone and coumarin derivatives. *Colloids Surfaces A Physicochem. Eng. Asp.* 127261.
- Salama, Reda S., El-Bahy, S.M., Mannaa, M.A., 2021a. Sulfamic acid supported on mesoporous MCM-41 as a novel, efficient and reusable heterogeneous solid acid catalyst for synthesis of xanthene, dihydropyrimidinone and coumarin derivatives. *Colloids Surfaces A Physicochem. Eng. Asp.* 628, 127261. <https://doi.org/10.1016/j.colsurfa.2021.127261>
- Salama, Reda S., El-Sayed, E.S.M., El-Bahy, S.M., Awad, F.S., 2021b. Silver nanoparticles supported on UiO-66 (Zr): As an efficient and recyclable heterogeneous catalyst and efficient adsorbent for removal of indigo carmine. *Colloids Surfaces A Physicochem. Eng. Asp.* 626, 127089. <https://doi.org/10.1016/j.colsurfa.2021.127089>
- Shi, Y., Wang, S., Ma, X., 2011. Microwave preparation of Ti-containing mesoporous materials. Application as catalysts for transesterification. *Chem. Eng. J.* 166, 744–750.

- Sudarsanam, P., Reddy, B.M., 2013. Production Techniques of Nanoparticles on a Laboratory Scale.
- Wang, X., Lian, W., Fu, X., Basset, J.-M., Lefebvre, F., 2006. Structure, preparation and photocatalytic activity of titanium oxides on MCM-41 surface. *J. Catal.* 238, 13–20.
- Zhang, X., Zhang, F., Chan, K.-Y., 2005. Synthesis of titania–silica mixed oxide mesoporous materials, characterization and photocatalytic properties. *Appl. Catal. A Gen.* 284, 193–198.